ACS APPLIED MATERIALS & INTERFACES

Research Article

www.acsami.org

Ultrasensitive Nanoporous Interferometric Sensor for Label-Free Detection of Gold(III) Ions

Tushar Kumeria, Abel Santos, and Dusan Losic*

School of Chemical Engineering, The University of Adelaide, Adelaide, South Australia, 5005, Australia

Supporting Information

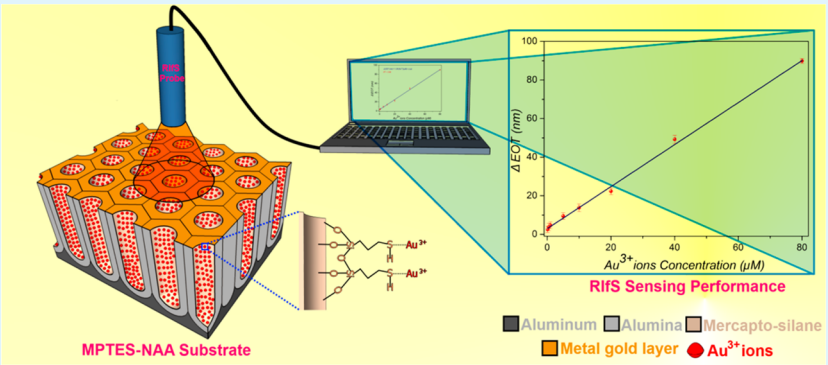

ABSTRACT: In this study, we present an ultrasensitive sensor based on nanoporous anodic alumina (NAA) for detection of gold(III) ions (Au^{3+} ions) using reflectometric interference spectroscopy (RIfS). Nanoporous anodic alumina, prepared by two-step electrochemical anodization, was functionalized with 3-mercaptopropyl-tirethoxysilane (MPTES) in order to selectively detect Au^{3+} ions. Thus prepared, MPTES-NAA sensors were exposed to different concentrations of Au^{3+} ions ranging from 0.1 to 750 μM and the changes in the effective optical thickness (ΔEOT) were monitored in real-time. The linear range of these Au^{3+} sensors was from 0.1 to 80 μM, with a lower detection limit of 0.1 μM of Au^{3+} ions. Furthermore, the specificity of these MPTES-NAA sensors was validated by sequential exposure to 40 μM solutions of Fe^{3+}, Mg^{2+}, Co^{2+}, Cu^{2+}, Ni^{2+}, Ag^{+}, and Pb^{2+}, resulting in negligible changes in EOT as compared to the same concentration of Au^{3+} ions. Detection of Au^{3+} ions in complex and environmentally and biologically relevant solvents such as tap water and phosphate buffer solution (PBS) was also successfully carried out in order to demonstrate the real-life application of these sensors. Finally, the binding isotherm for Au^{3+} ions and thiol (SH) group of MPTES-NAA system was determined by fitting the changes in EOT to Freundlich and Langmuir isotherm models.

KEYWORDS: *nanoporous anodic alumina, reflectometric interference, gold(III) ions, optical sensing, chemical functionalization*

1. INTRODUCTION

In the past decade, the use of gold and gold-based salts has grown very rapidly because of its unique properties (e.g., chemical activity, stability, ability to form functional nanoparticles, etc.). In particular, gold and its salts play key roles in mining, mineral processing, chemistry, medicine, electronics, and biology. For instance, gold is employed in chemistry for catalysis and synthesis of nanomaterials such as nanowires, nanotubes, nanorods, and nanomembranes.[1−4] Gold is a basic element used in many critical components of electronic devices as it fulfills all the electronic requirements better than any other metal (e.g., high corrosion resistance, thermal stability, electrical conductivity, etc.). It is worth stressing that these electronic devices expose these gold-based components to environmental conditions in two ways: either during processing/manufacturing or at the end of their life-cycle, when they are deposited in the dump yard. Under these conditions, gold can leach to soil and underground water by several ways.[5,6] Another important application of gold is in medicine where gold-based drugs are used to treat a broad variety of diseases, including asthma, malaria, cancer, HIV, arthritis, and brain lesions.[7−10] Moreover, gold nanoparticles obtained by reduction of gold ions are used for sensing, drug/gene delivery, and bioimaging.[11−14] Notice that metallic gold is proven to be highly biocompatible and considerably stable in biological conditions.[15,16] Nevertheless, some studies have demonstrated that metallic gold can be chemically oxidized to ionic states by strong oxidants, which are present in environmental and biological conditions.[17,18] These ionic gold species (i.e., Au^{+} and Au^{3+}) are highly reactive and potentially toxic to humans.[19] As for this, it is worth noting that gold salts such as gold chloride cause serious damage to liver, kidneys, and the peripheral nervous system.[20] Particularly, Au^{3+} ions, which are known to bind tightly to DNA and several enzymes leading to DNA cleavage, can degenerate into

Received: August 17, 2013
Accepted: October 14, 2013
Published: October 14, 2013

Scheme 1. Schematic Diagram of RIfS-NAA Sensing System for Detection of Gold Ions on Mercapto-Silane Modified Nanoporous Anodic Alumina[a]

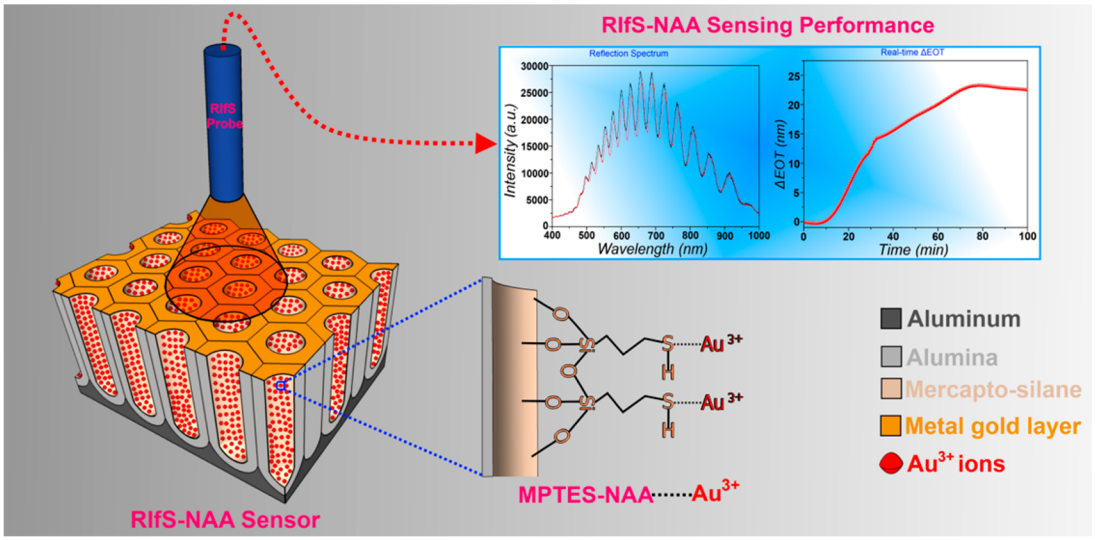

[a]An optical fiber probe shines light on the MPTES-NAA substrate surface to obtain reflective interference fringe pattern and real-time RIfS response curve for Au^{3+} ions detection.

disruption of nervous systems.[21,22] In addition, cytotoxicity of gold nanoparticles to human cells is also a debatable issue.[23]

Therefore, since the use of gold species, in ionic or nanoparticle form, is on the rise in medicine, mining, mineral processing, chemical, electronic, and catalysis industries, more efficient, accurate, sensitive, cost-competitive, and versatile detection systems must be implemented in order to address the toxic effects associated with different gold species present in environmental and biological samples (e.g., water or blood). Traditionally, heavy metals, including gold species, are detected by means of analytical techniques such as UV−visible and fluorescence spectroscopy, atomic absorption spectroscopy (AAS), atomic fluorescence microscopy (AFS), and inductively coupled plasma mass spectroscopy (ICP-MS).[24] Recently, surface plasmon resonance (SPR) and photoluminescence spectroscopy (PLS) have also been extensively applied in detection of gold species by means of several specific probes by taking advantage of alkynophilicity of gold.[21,22,26−30] Although these techniques provide highly sensitive analyses, they require complex and time-consuming sample preparation steps in addition to expensive and sophisticated instrumentation, skilled operators, large sample volume, destruction of sample, and inability to do real-time measurements.[25] Consequently, new sensing methods are required for overcoming the above-mentioned drawbacks and developing ultrasensitive and fast gold sensors for environmental and biological applications.

In this scenario, optical detection methods have emerged as an outstanding alternative as a result of their high sensitivity, low cost, real-time and point-of-care detection, and ease of miniaturization.[31,32] Thus, a label-free sensing platform for real-time detection of gold(III) ions is considered to be an attractive alternative to current sensing techniques used to detect gold ions. Among these optical techniques, reflectometric interference spectroscopy (RIfS) is a simple optical method of detection based on thin film interference of white light.

The principle of RIfS is the Fabry−Pérot interference phenomenon, which results in appearance of alternate fringe maxima and minima (i.e., fringes) in the reflection spectrum when white light is reflected from top and bottom interfaces of an air-thin film system.[33] Notice that these well-resolved fringes follow the Fabry−Pérot relationship (eq 1), from which the effective optical thickness (EOT) can be calculated.

$$\mathrm{EOT} = m\lambda = 2n_{\mathrm{eff}}L \tag{1}$$

where m is the fringe order in the RIfS spectrum, of which the maximum is located at the wavelength λ, n_{eff} is the effective refractive index of the film, and L its physical thickness. Therefore, any change in n_{eff} or L results in a variation in the fringe pattern (i.e., shift of fringes in the RIfS spectrum) and thus a change in the optical thickness, which forms the basis of RIfS sensing system.[31,33] Thus far, many studies have reported about the RIFs based detection of a broad range of analytes (e.g., proteins, antigens, environmental pollutants, tumor cells, organic compounds, etc.) by using thin polymer films or inorganic nanoporous films (e.g., porous silicon, nanoporous alumina, and nanotubular titania).[34−41] In particular, integration of RIfS with nanoporous substrates results in improvement of sensing characteristics as these nanopores act as containers for analytes, enhancing the optical signal from the analyte molecules immobilized onto these nanoporous films.[42−44] As for this, nanoporous anodic alumina (NAA) provides highly controllable and designable porous geometry, tunable surface chemistry, biocompatibility, chemical and thermal stability, easy and scalable fabrication process, and stable optical activity.[45] These properties make NAA as an emerging and outstanding substrate for RIfS sensing.[45] NAA-based RIfS sensing platforms have already been proven for highly sensitive and specific detection of proteins/antibodies, volatile organic/sulfur compounds (e.g., ethanol, acetone, hydrogen sulfide, etc.), nucleic acids (DNA), and circulating tumor cells.[31,38,40,43−46] However, to the best of our knowledge, so far no study has reported about the detection of gold ions using RIfS or any other sensing technique combined with NAA substrates.

Herein, we present a highly sensitive, selective, and label-free optical sensor for detection of gold(III) ions (Au^{3+} ions) on mercapto-silane modified NAA combined with RIfS. NAA

prepared by two-step electrochemical anodization was functionalized with 3-mercaptopropyl-tirethoxysilane (MPTES) to impart gold specific thiol terminal groups throughout the inner surface of pores. MPTES modified NAA samples (MPTES-NAA) were then used to detect different concentrations of Au^{3+} ions. The proposed detection concept for Au^{3+} ions along with the characteristic optical interference pattern and real-time sensing signal are presented in Scheme 1. Selectivity and specificity of MPTES-NAA system to detect Au^{3+} ions was established by measuring its RIfS response on exposure to solutions composed of different metal ions (Fe^{3+}, Mg^{2+}, Co^{2+}, Cu^{2+}, Ni^{2+}, Ag^{+}, and Pb^{2+}). In addition, MPTES-NAA was exposed to three binary mixtures of Ag^{+}, Pb^{2+}, and Au^{3+} to further prove the selectivity of MPTES-NAA system toward Au^{3+} ions. Lastly, detection of Au^{3+} ions in tap water and phosphate buffer solution (PBS) was carried out to prove the real-life application of the proposed MPTES-NAA-based RIfS sensing device.

2. EXPERIMENTAL SECTION

2.1. Materials. Aluminum (Al) foil (thickness 0.3 mm, purity 99.9997%) was supplied by Goodfellow (Germany). Oxalic acid ($C_2H_2O_4$), ethanol (C_2H_5OH), acetone ($(CH_3)_2CO$), perchloric acid ($HClO_4$), hydrogen peroxide (H_2O_2), chromium trioxide (CrO_3), 3-(mercaptopropyl)-triethoxysilane (MPTES), silver(I) nitrate ($AgNO_3$), copper(II) chloride ($CuCl_2$), magnesium(II) chloride ($MgCl_2$), lead(II) nitrate ($Pb(NO_3)_2$), cobalt(II) chloride ($CoCl_2$), nickel(II) sulfate ($NiSO_4$), iron(III) chloride ($FeCl_3$), and gold(III) chloride ($AuCl_3$) were purchased from Sigma Aldrich (Australia) and used without further processing. Ultrapure water was used for preparation of all solutions used in this study (Option Q, Purelabs, Australia).

2.2. Preparation of NAA Substrates. Nanoporous anodic alumina sensor substrates were prepared by anodizing high purity Al foils by a two-step electrochemical anodization process reported previously.[39,47] Briefly, circular chips of Al with diameter 1.5 cm were first sonicated in ethanol (EtOH) and distilled water for 15 min each, followed by drying under nitrogen stream. Aluminum chips were electropolished prior to anodization in a mixture of ethanol (EtOH) and perchloric acid ($HClO_4$) 4:1 (v:v) at 20 V and 5 °C for 3 min. These electropolished Al chips were then subjected to two-step anodization. The first anodization step was carried out in a 0.3 M aqueous solution of oxalic acid ($H_2C_2O_4$) at 40 V and 6 °C for 20 h. This was followed by removal of the resulting NAA layer using wet chemical etching in solution of 0.2 M chromic acid (H_2CrO_4) and 0.4 M phosphoric acid (H_3PO_4) at 70 °C for 3 h. Finally, the second anodization step was performed for 70 min under the same conditions (i.e., 0.3 M $H_2C_2O_4$, 40 V, and 6 °C). This anodization step was controlled specifically to yield NAA which satisfies all mathematical and structural requirements for generating an optimized reflective interference spectrum.[39]

2.3. Mercapto-Silanization of NAA. NAA substrates were modified with 3-(mercaptopropyl)-triethoxysilane (MPTES) in order to obtain thiol terminal groups over the inner surface of the NAA pores. Silanization was carried out using a well-established protocol reported elsewhere.[48] Briefly, NAA samples fabricated by two-step anodization were first treated with hydrogen peroxide solution (H_2O_2) 30 wt % for 10 min at 85 °C and dried under nitrogen stream to increase the number of hydroxyl groups on their surface. Next, these hydroxylated NAA samples were functionalized by chemical vapor deposition of MPTES at 135 °C for 3 h. After that, MPTES functionalized NAA samples were thoroughly washed with acetone and water to remove any physisorbed MPTES molecules and dried under nitrogen stream. Next, prepared MPTES-NAA sensing platforms were coated with an ultrathin film of gold (i.e., 4−5 nm) using a sputter coater equipped with film thickness monitor (sputter coater 108auto, Cressington, USA) to enhance the refractive index contrast and stored in a desiccator under vacuum until further use to prevent oxidation of thiol terminal groups. Successful silanization was proven by using Fourier transform infrared spectroscopy (FTIR, Nicolet 6700, ThermoFisher, Australia) in the spectral range from 1000 to 3500 cm^{-1}.

2.4. RIfS System and Detection of Au^{3+} Ions. Details of the optical setup used for RIfS monitoring has been provided in our previous works.[31,41] Briefly, white light from a tungsten source (LS-1LL, Ocean Optics, USA) is carried by one arm of a bifurcated optical probe and directed onto MPTES-NAA sensing surface through its common arm, with an illumination spot of 2 mm in diameter. The reflected light from this spot is collected by the collection fiber assembled in the same optical probe and transferred to a miniature spectrophotometer (USB 4000, Ocean Optics, USA). UV−visible optical spectra were acquired in the 400−1000 nm wavelength range during the detection of Au^{3+} ions. Spectral data were saved at intervals of 30 s with an integration time of 100 ms and 50 average measurements (i.e., time between two consecutive scans = 5 s). Thus collected, reflectometric interference optical spectra were processed by applying fast Fourier transform (FFT; Igor Pro library, Wavemetrics, USA) to obtain the EOT. EOT was used as the sensing parameter, and its changes were monitored in real-time to follow the binding of Au^{3+} ions to thiol groups of MPTES functionalities inside the NAA pores.

A stock solution of Au^{3+} ions (1 mM) was prepared from $AuCl_3$ in ultrapure water, which was further diluted to obtain the required different concentrations of Au^{3+} ions. Twelve different concentrations of Au^{3+} ranging from 0.1 to 750 μM were prepared and subsequently used for studying the sensing performance of the proposed sensors. Sensing experiments were carried out by packing the ultrathin gold coated MPTES-NAA samples in a custom designed and fabricated flow cell. All the real-time sensing measurements in the flow cell were carried out at a flow rate of 200 $\mu L\ min^{-1}$, which was maintained using a syringe pump (Fusion touch, Chemyx, USA). A stable baseline with ultrapure water was established for 10 min prior to injection of the different analyte solutions into the flow cell. The contact of Au^{3+} ions with thiol groups on MPTES-NAA produced changes in EOT and continued until all the thiol groups on the NAA surface were saturated with Au^{3+} ions. To prove that these changes in EOT are a result of selective binding of Au^{3+} ions with thiol groups on MPTES-NAA, a control tests was carried out by exposing an unmodified NAA (i.e., NAA without MPTES functionalization) to 20, 40, and 80 μM Au^{3+} solutions. Selectivity of the proposed MPTES-NAA sensing platform toward Au^{3+} ions was established by exposing MPTES-NAA sensor to solutions of seven different metal ions (40 μM Fe^{3+}, 40 μM Mg^{2+}, 40 μM Co^{2+}, 40 μM Cu^{2+}, 40 μM Ni^{2+}, 40 μM Ag^{+}, and 40 μM Pb^{2+}) followed by a twofold lower concentration of Au^{3+} ions (20 μM). Furthermore, to determine the selectivity of the MPTES-NAA sensing system, we exposed these sensors to three different model solutions containing different interfering analytes prepared by mixing 40 μM solutions of selected ions. (i) Mix-1: Pb^{2+} and Ag^{+} (1:1 v:v, 40 μM Pb^{2+}/40 μM Ag^{+}). (ii) Mix-2: Au^{3+} and Pb^{2+} (1:1 v:v, 40 μM Au^{3+}/40 μM Pb^{2+}). (iii) Mix-3: Au^{3+} and Ag^{+} (1:1 v:v, 40 μM Au^{3+}/40 μM Ag^{+}). So, the final concentration of each individual metal ion in these mixed solutions was 20 μM. Finally, to check the real-life application of the proposed sensing platforms, MPTES-NAA substrates were subjected to detection of Au^{3+} ions (40 μM) in tap water and PBS. Notice that all the above-mentioned experiments were repeated three times using three freshly prepared MPTES-NAA sensors and statistically analyzed by calculating averages and standard deviations.

2.5. Isotherms for Binding of Au^{3+} Ions to MPTES-Modified NAA. Langmuir and Freundlich isotherm models were used to establish the kinetics binding mechanism of Au^{3+} ions onto thiol groups of MPTES-modified NAA sensors.[42] The Langmuir isotherm is given by eq 2.

$$\frac{[Au^{3+}]}{\Delta EOT_e} = \frac{1}{K_L \Delta EOT_m} + \frac{[Au^{3+}]}{\Delta EOT_m} \quad (2)$$

where $[Au^{3+}]$ is the concentration of Au^{3+} ions, ΔEOT_e is the change in EOT at equilibrium, and K_L and ΔEOT_m are characteristic

constants. Parameters $1/K_L\Delta EOT_m$ and $1/\Delta EOT_m$ can be obtained by the intercept and slope of a plot between $[Au^{3+}]/\Delta EOT_e$ and $[Au^{3+}]$, respectively.

As for the Freundlich isotherm, this is given by eq 3.

$$\log(\Delta EOT_m) = \log K_f + \frac{1}{n}\log[Au^{3+}] \quad (3)$$

where ΔEOT_e is the change in EOT at equilibrium, $[Au^{3+}]$ is the concentration of Au^{3+} ions, and K_f and n are characteristic constants. Values of log K_f and $1/n$ can be determined, respectively, by the intercept and slope of a plot between $\log(\Delta EOT_e)$ and $\log[Au^{3+}]$. Mathematical derivation for all the above equations is provided in the Supporting Information.

3. RESULTS AND DISCUSSION

3.1. Structural Characterization and Chemical Analysis of NAA. As reported previously, the structural characteristics of NAA are critical to its reflective interference properties and sensing performance.[39] Scanning electron microscopy (SEM) imaging was performed to confirm that desired nanoporous layer was obtained. Figure 1 shows typical SEM images of NAA structure prepared by the two-step electrochemical anodization process. Figure 1a presents a SEM image of top surface of NAA, which clearly shows hexagonally organized pores with diameters of 35 ± 5 nm with an inset digital photograph of an NAA sensor. SEM characterization performed after MPTES modifications inside nanopores and gold deposition on the top NAA surface did not show any change in the pore geometry (Figure S1, Supporting Information). The cross-sectional SEM image of NAA provided in Figure 1b reveals perfectly straight and vertically aligned cylindrical pores, which are closed at the bottom side by an oxide barrier layer. The pore length in the resulting NAA samples was 4.5 ± 0.2 μm, which is an optimal length for RIfS in accordance with our previous work.[39]

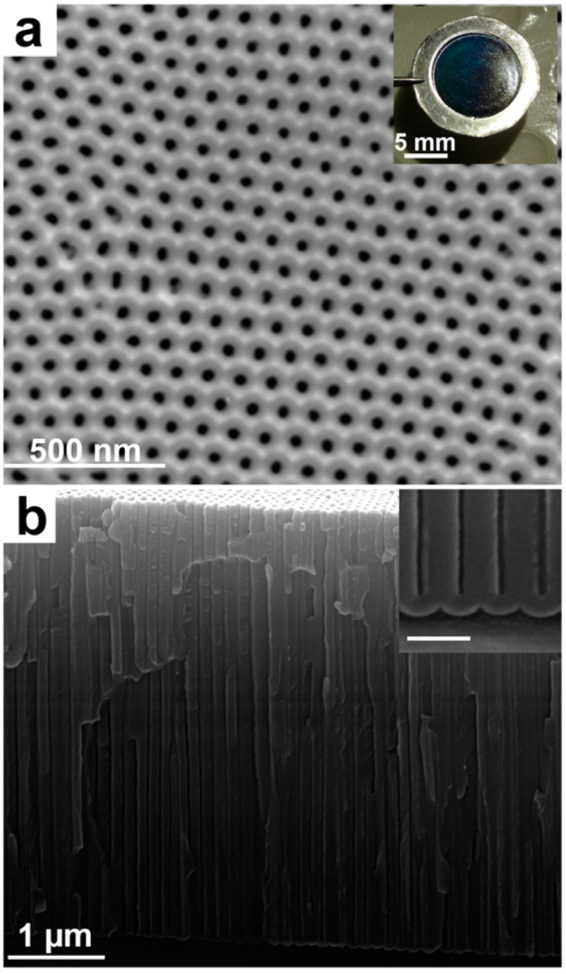

Figure 1. SEM images of typical NAA substrates used for RIfS Au^{3+} ions sensing. (a) Top view showing hexagonally arranged pores with inset digital photograph of MPTES-NAA sensor. (b) Cross-sectional view of the same NAA sample with straight cylindrical pores with inset image showing closed pores at the bottom by an oxide barrier layer (scale bar = 100 nm).

These NAA samples were modified with MPTES to obtain thiol functional groups on the alumina surface for specific detection of gold(III) ions. FTIR spectroscopy data shown in Figure 2 prove the silanization of NAA. Whereas FTIR peaks at

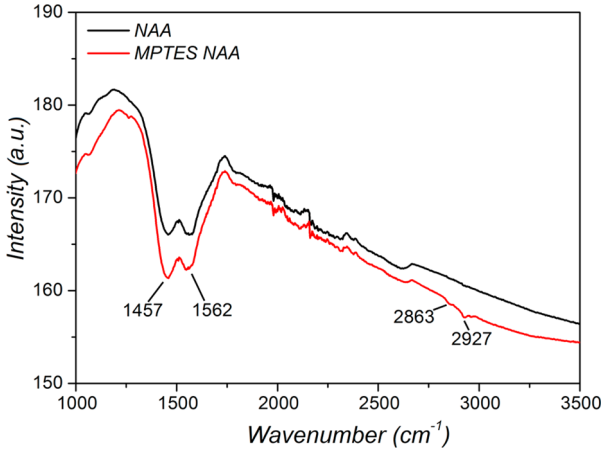

Figure 2. FTIR spectra of as-produced NAA and MPTES modified NAA.

1460 and 1570 cm^{-1} are associated with nanoporous anodic alumina, the appearance of additional peaks at 2929 and 2869 cm^{-1} corresponds to asymmetric and symmetric vibrations of methylene ($-CH_2-$) group of propyl chain, respectively. This confirms the presence of thiol terminal groups of MPTES molecules on the NAA surface.[49,50] Furthermore, SEM images obtained after MPTES surface functionalization and ultrathin gold coating show that the NAA samples maintain their porous structure (Figure S1, Supporting Information).

3.2. Detection of Au^{3+} Ions on MPTES-Modified NAA. NAA modified with MPTES was used as a sensing substrate for detection of Au^{3+} ions. Figure 3a shows a typical example of interference pattern obtained by shining white light on MPTES-NAA surface. This figure also shows the red-shift of the interference fringe pattern on exposure of MPTES-NAA sensor chip to Au^{3+} ions ($[Au^{3+}]$ = 40 μM). To resolve this red-shift in interference pattern, FFT was applied and EOT calculated. This parameter (EOT) was used as the sensing parameter for detection of Au^{3+} ions. Figure 3b presents a real-time monitoring plot of ΔEOT by RIfS using a MPTES-NAA sensor for detection of 20 μM Au^{3+} ions solution in ultrapure water. Notice that, as was mentioned previously, a stable ΔEOT baseline was first obtained with ultrapure water for 10 min followed by injection of the analyte solutions. When this MPTES-NAA sample was exposed to the analyte solution, a rapid and sharp increase was observed initially, which slowed down progressively to achieve a stable value of 24 nm in

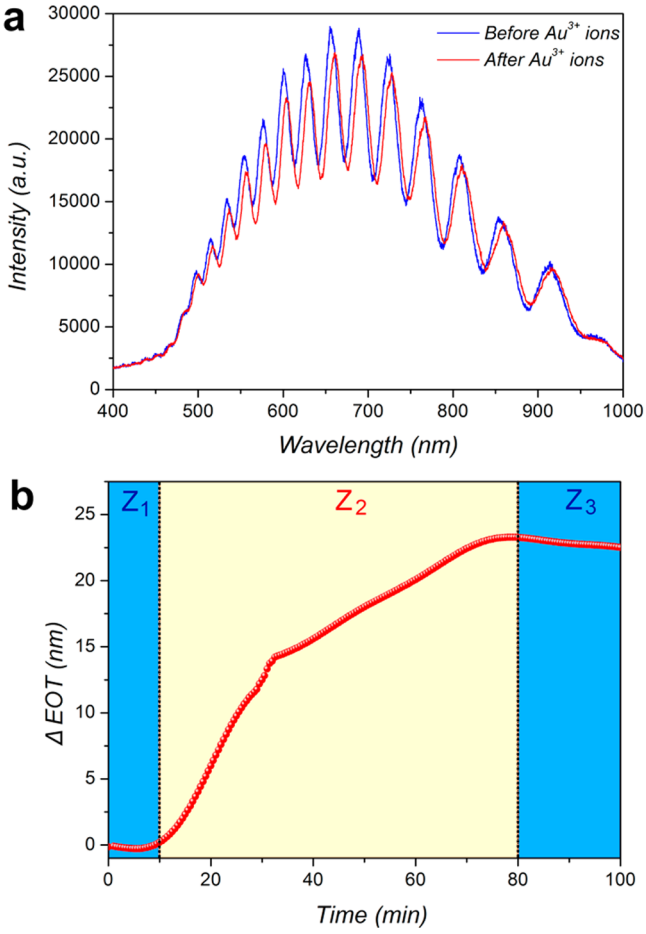

Figure 3. Detection performance of Au^{3+} ions by RIfS using the proposed MPTES-NAA sensor. (a) Optical interference spectrum of MPTES-NAA sensor before and after exposure to gold(III) ions. (b) Real-time detection curve of 20 μM Au^{3+} ions solution in ultrapure water consisting of three zones: (Z_1) ultrapure water for baseline; (Z_2) 20 μM aqueous solution of Au^{3+} ions; and (Z_3) rinse with ultrapure water.

ΔEOT. This confirmed the attachment of Au^{3+} ions to thiol terminals of MPTES molecules present on the surface inside NAA pores. It is worthwhile mentioning that after achieving the equilibrium ΔEOT value, on rinsing the MPTES-NAA sensor with ultrapure water, the observed ΔEOT value decreased slightly to 22 nm and remained stable throughout. This slight decrease and formation of another baseline at 22 nm in ΔEOT is associated with the removal of nonspecifically bound Au^{3+} ions. Similar trend in ΔEOT was observed in all the concentrations above 5 μM, while lower concentrations showed a more linear trend with time. Therefore, the total increase in ΔEOT is a result of an increase in the effective refractive index of the effective medium (i.e., MPTES-NAA sensor) related to the stable attachment of Au^{3+} ions on the inner surface of NAA pores. Notice that the average response time of the proposed RIfS-based gold(III) ions sensor to reach 90% (t_{90}) of the stable ΔEOT value was 40 ± 8 min for all the measured Au^{3+} ion concentrations (0.1−750 μM), which is either comparable or better than the response times of fluorescence and SPR-based metal ion detection systems. Furthermore, we also observed that the time required for ΔEOT to reach the equilibrium value increased by decreasing the concentration of Au^{3+} ions in analyte solutions.

The sensor performance as a function of the analyte concentration is shown in Figure 4a. This calibration curve

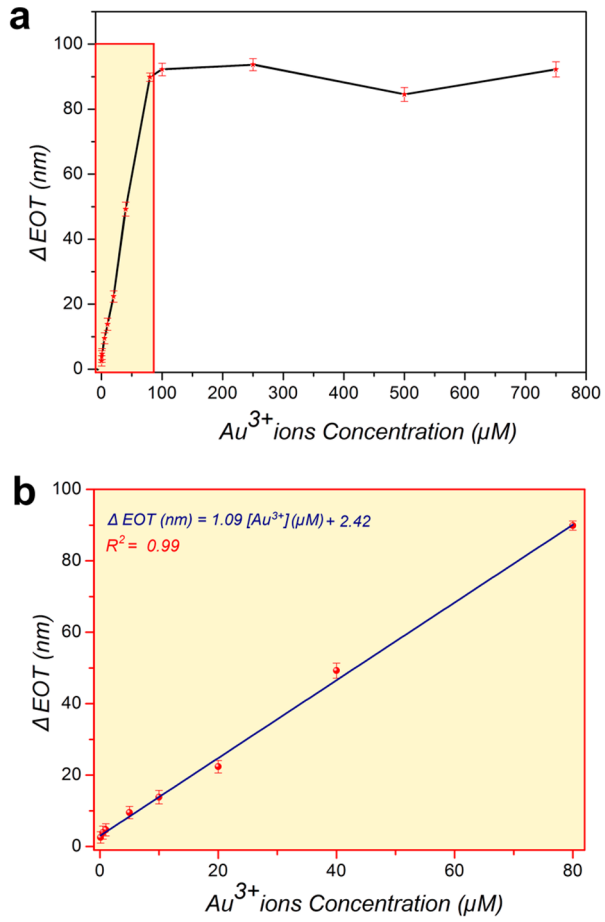

Figure 4. (a) ΔEOT as a function of the concentration of Au^{3+} ions on MPTES-NAA sensors throughout the complete concentration range of 0.1−750 μM. (b) Magnified view of red rectangle (yellow background) shown in (a), which corresponds to the calibration curve for the linear range of Au^{3+} ions detection.

obtained from RIfS measurements correlates the effective optical thickness change and the concentration of gold(III) ions in the analyte solution. Twelve different concentrations in a broad range of 4 orders of magnitude (i.e., 0.1−750 μM) of Au^{3+} ions were analyzed in order to characterize linear and saturation range of the proposed MPTES-NAA sensing device. Figure 4a clearly shows that ΔEOT value tends to saturate at concentrations above 80 μM. This suggests saturation of all possible binding sites (i.e., thiol terminal groups) for Au^{3+} ions on the MPTES-NAA substrate. A linear relationship between ΔEOT and Au^{3+} ions concentration was observed within the concentration range of 0.1−80 μM (i.e., 0.019−15.736 ppm (ppm = parts per million)), which is presented in Figure 4a (red rectangle). A linear regression fit of the linear range is presented in Figure 4b along with the resulting fitting equation. This calibration curve can be used to quantify the concentration of Au^{3+} ions in an aqueous solution from the effective optical thickness change provided by the proposed sensing platform. Notice that this result demonstrates that qualitative analyses to determine the presence/absence of gold(III) ions in the sample are possible within the studied concentration range (i.e., 0.1−750 μM) using the proposed MPTES-NAA sensor. However,

dx.doi.org/10.1021/am403465x | ACS Appl. Mater. Interfaces 2013, 5, 11783−11790

quantitative detection of gold(III) ions can only be performed in the concentration range 0.1 to 80 μM. The dynamic linear range of the proposed sensor is very broad (i.e., 0.1−80 μM: three orders of magnitude in concentration) which is better than that of most gold(III) ion sensors reported previously.[26−29] Furthermore, a linear relation between Au^{3+} concentration and change in EOT can be obtained 25 min after starting the Au^{3+} ion measurement, showing a reasonable analytical performance for a concentration range of 0.1−80 μM of gold(III) ions (Figure S2, Supporting Information).

It is worth noting that this MPTES-NAA-based RIfS detection system was able to detect 0.1 μM of Au^{3+} ions in aqueous solution, with a limit of detection (LOD) lower than 0.1 μM. Hence, the LOD of the proposed RIfS sensing system is lower than that of most of the previously reported fluorescence-based systems for quantifying Au^{3+} ions.[26−29] This detection limit depends on several parameters and can be improved by several ways: by increasing the density of binding SH groups on the pore surface by surface functionalization using organic compounds consisting multiple mercapto groups (i.e., −SH) or by further optimization of the pore structure by increasing the active surface area and enhancing the optical signal and by structural engineering of NAA sensor chip. Mercapto-silane functionality was specifically chosen because the thiol functional group is known to bind selectively and specifically to certain metal ions, including Au^{3+} ions. A control experiment was carried out in order to confirm the selective binding of Au^{3+} ions through thiol groups on MPTES-NAA. To this end, an unmodified NAA substrate (i.e., without mercapto-silane) was consecutively exposed to 20, 40, and 80 μM aqueous solutions of gold(III) ions (Figure S3, Supporting Information). A change in EOT of approximately 5.78, 6.45, and 6.71 nm was observed for 20, 40, and 80 μM aqueous solutions of Au^{3+} ions, respectively. Notice that, when exposed to 20 μM, 5.78 nm change in EOT was observed, while subsequent subjection to 40 and 80 μM only resulted in 6.45 and 6.71 nm of change in EOT, respectively. This could be explained by nonspecific and fast adsorption of Au^{3+} ions onto inherently negatively charged NAA.

3.3. Selectivity of MPTES-NAA toward Au^{3+} Ions. Selectivity of the proposed MPTES-NAA system was analyzed by two sets of experiments. First, a selectivity test was carried out by exposing a MPTES-NAA sensor to 40 μM aqueous solutions of Fe^{3+}, Mg^{2+}, Co^{2+}, Cu^{2+}, Ni^{2+}, Ag^{+}, and Pb^{2+} ions in a succession followed by 20 μM Au^{3+} ions. These interfering metal ions are selected as common ions in natural water solutions and ions that have low (Fe, Mg) and high (Ag) affinity toward mercapto groups. Figure 5 shows a bar graph plot of ΔEOT for the aforementioned aqueous ionic solutions. The highest nonspecific change in EOT was observed for Ag^{+} and Pb^{2+} analytes (~5.67 and 5.63 nm, respectively) followed by Mg^{2+}, Ni^{2+}, Co^{2+}, Fe^{3+}, and Cu^{2+}. However, when the same sample was exposed to a 20 μM aqueous solution of Au^{3+} ions, a significant change in EOT of more than 20 nm was observed. This result proves that the MPTES-NAA sensor is highly selective toward gold(III) ions.

The second selectivity test was carried out by exposing the MPTES modified NAA sensor to a 1:1 mixture of Pb^{2+} and Ag^{+} (i.e., mix-1), Au^{3+} and Pb^{2+} (i.e., mix-2), and Au^{3+} and Ag^{+} (i.e., mix-3) (Figure 5). Exposure of the MPTES-NAA sensor to mix-1 resulted in a practically negligible RIfS response (i.e., EOT change) of approximately 5.47 nm, while mix-2 and mix-3 resulted in approximately 21.23 and 22.41 nm, respectively.

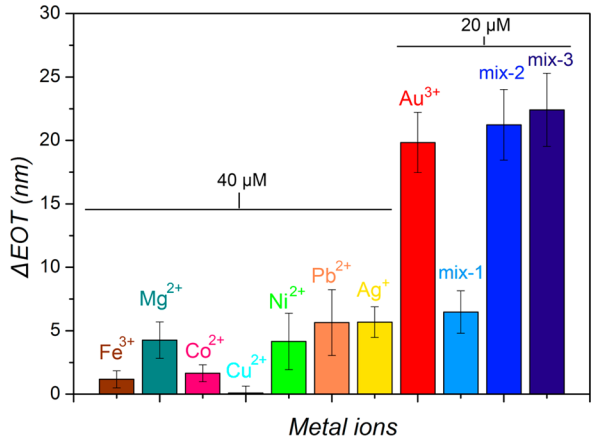

Figure 5. Bar graph chart showing the effective optical thickness change of the proposed RIfS sensing system based on MPTES modified NAA sensor after exposure to several aqueous metal ion solutions, the concentration of which was 2 times (40 μM) higher than that for Au^{3+} ions, which was 20 μM, and different binary mixtures (i.e., mix-1: Pb^{2+} and Ag^{+}, mix-2: Au^{3+} and Pb^{2+}, and mix-3: Au^{3+} and Ag^{+}) having a 20 μM final concentration of each metal ion in each mix.

These results again demonstrate the capability of the proposed RIfS system based on NAA functionalized with specific ligands, which has an outstanding performance for label-free and highly selective detection of gold(III) ions even in solutions composed of multiple metal ions. These results motivated us for detecting gold(III) ions in complex solvents as tap water and phosphate buffer solution in order to explore its practical applications.

3.4. Detection of Au^{3+} Ions in Environmental and Biological Scenarios. To analyze the performance of the proposed optical RIfS sensor in a real-life application, a 40 μM solution of gold(III) ions was prepared in tap water and phosphate buffer solution. The 40 μM solution of gold(III) ions prepared in ultrapure water was used as a control. As for RIfS measurements for an environmental sample as tap water, first, a baseline was obtained with tap water followed by injection of gold(III) ions solution prepared in tap water. Similarly, for detection of gold(III) ions in a biological environment, a baseline with PBS was first obtained for 10 min and then a 40 μM solution of gold(III) ions in PBS was flowed. RIfS response for gold(III) ions in tap water and PBS was found to be approximately 42.85 and 44.83 nm, respectively. This response is slightly lower in comparison to 49.28 nm for the same concentration of gold(III) ions in ultrapure water (Figure 6). This lower response and higher standard error can be associated with the number of nonspecific adsorption of other ionic species present in these complex solutions (i.e., tap water and PBS) and reduced actual concentration of Au^{3+} ions due to their interaction with impurities and compounds present in these complex solvents, which reduce their binding affinity toward thiol group. In addition, a real-time RIfS response curve for 40 μM Au^{3+} ions in ultrapure water and tap water is provided in Figure S4 (Supporting Information), showing that the latter presented a more noisy signal compared to the former. This can be ascribed to the presence of various metallic, ionic, molecular, and organic impurities present in tap water. Therefore, the proposed MPTES-NAA sensor proved its capability for label-free detection of gold(III) ions in real-life samples.

3.5. Binding Isotherms for Au^{3+} Binding to Thiol Groups of MPTES-NAA. Langmuir and Freundlich binding

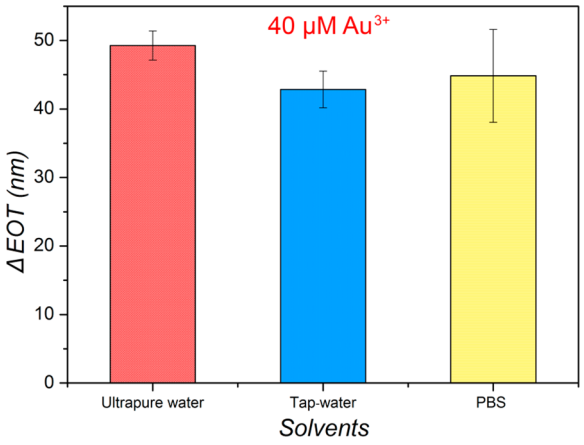

Figure 6. RIfS response on exposing a MPTES-NAA sensor to 40 μM Au^{3+} ions solution prepared in ultrapure water, tap water, and PBS.

isotherm models were used to describe the binding mechanism of Au^{3+} ions onto thiol groups present on the MPTES-modified surface of NAA. These data were fitted to the aforementioned eqs 2 and 3 (Experimental Section) to discern which of these binding isotherms explains the binding mechanism of gold(III) ions in the proposed optical sensors. On the one hand, the Langmuir isotherm is more suitable for flat surfaces and it considers the number of binding sites to be constant throughout the reaction. On the other hand, the Freundlich isotherm is a more suitable model for binding on rough surfaces and it assumes that the binding sites increase with the concentration of analyte molecules (i.e., $[Au^{3+}]$). The calculated constant values for both isotherm models and their corresponding correlation factors are given in Table 1. These

Table 1. Characteristic Constants and Correlation Coefficients for Langmuir and Freundlich Binding Isotherms for Detection of Gold(III) Ions in the Proposed Optical Biosensors

Langmuir isotherm			Freundlich isotherm		
ΔEOT_m (nm)	K_L (μM^{-1})	R^2	n	K_f	R^2
94.34	3.70×10^{-2}	0.99	2.05	5.75	0.93

results denote that the binding mechanism of gold(III) ions to the thiol groups present on the sensor surface follows a Langmuir isotherm model, which has a better fitting than Freundlich isotherm, according to the R^2 values.

Figure 7 presents a graphic of the obtained Langmuir and Freundlich isotherms along with the experimental data, which were observed to fit better to a Langmuir isotherm model with a fitting efficiency of 93% in comparison to 61% of a Freundlich isotherm model. This suggests that the attachment of Au^{3+} ions is similar to monolayer sorption, which was expected as the number of binding sites in the sensing platform remains constant throughout and the inner surface of pores in NAA is flat and fairly smooth.

Therefore, the above-mentioned results have demonstrated the application of MPTES-NAA chips for capturing and label-free detection of gold(III) ions with a broad linear range and a low limit of detection in ultrapure water and complex solvent systems such as tap water and PBS.

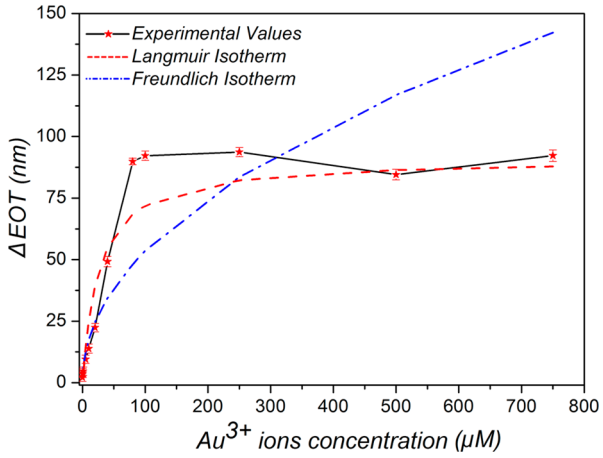

Figure 7. Langmuir and Freundlich binding isotherm fittings and experimental values for binding of Au^{3+} ions to thiol groups on MPTES modified NAA surface.

4. CONCLUSIONS

In summary, we have demonstrated the capability of reflective interference spectroscopy combined with nanoporous anodic alumina substrates modified with mercaptro-silane to carry out label-free detection of gold(III) ions. Gold(III) ion solutions with a broad range of concentrations (i.e., 0.1−750 μM) were detected on these optical sensors. The linear detection range of the proposed system was measured to be 0.1−80 μM with a lower limit of detection of 0.1 μM. Highly selective detection of gold(III) ions was achieved through thiol functionalities on MPTES-NAA, which showed negligible RIfS response on exposure to aqueous solutions of Fe^{3+}, Mg^{2+}, Co^{2+}, Cu^{2+}, Ni^{2+}, Ag^{+}, and Pb^{2+} ions (at 40 μM concentration). Furthermore, the RIfS-MPTES-NAA sensing system was capable of selectively detecting gold(III) ions in binary mixtures of different metal ions (i.e., 1:1, 40 μM/40 μM, Pb^{2+} and Ag^{+}, Au^{3+} and Pb^{2+}, and Au^{3+} and Ag^{+}). The real-life application of this RIfS-based sensing platform for detection of gold(III) ions was proven by successful detection of 40 μM Au^{3+} ions in tap water and PBS. At last, the fitting results for binding isotherms reveal that the binding mechanism of gold(III) ions to thiol terminals inside the NAA pores follows a Langmuir isotherm model. In this study, gold(III) ions have been used as a model ion but the proposed RIfS sensing system based on NAA can be considered as a generic concept as it can be modified at will by changing the surface chemistry (i.e., chemical ligand) on the surface inside the NAA pores. Therefore, the proposed sensors can be used to selectively detect any other metal ion, including heavy and toxic metal ones, which are of high interest for environmental control and biomedical applications.

■ ASSOCIATED CONTENT

Supporting Information

Further details about SEM images of NAA after MPTES-silanization, real-time response curves for concentrations in linear detection range and calibration curve for fast measurements, control experiment with unmodified NAA, and Langmuir and Freundlich binding isotherm models. This material is available free of charge via the Internet at http://pubs.acs.org.

AUTHOR INFORMATION

Corresponding Author

*E-mail: dusan.losic@adelaide.edu.au.

Author Contributions

The manuscript was written through contributions of all authors. All authors have given approval to the final version of the manuscript.

Notes

The authors declare no competing financial interest.

ACKNOWLEDGMENTS

Authors acknowledge the financial support provided by the Australian Research Council (DP 120101680, FT 110100711) and the School of Chemical Engineering − The University of Adelaide. We are also thankful to Prof. M. J. Sailor (UCSD) for providing FFT analysis software. We thank the workshop staff from the School of Chemical Engineering, particularly Mr. Jason Peak, Mr. Michael Jung, and Mr. Jeffrey Hiorns, for assistance with the fabrication of the flow cell for RIfS.

REFERENCES

(1) Rosi, N. L.; Mirkin, C. A. *Chem. Rev.* **2005**, *105*, 1547−1562.
(2) Wang, Z.; Ma, L. *Coord. Chem. Rev.* **2009**, *253*, 1607−1618.
(3) Li, Z.; Brouwer, C.; He, C. *Chem. Rev.* **2008**, *108*, 3239−3265.
(4) Gorin, D. J.; Toste, F. D. *Nature* **2007**, *446*, 395−403.
(5) Ishikawa, S.; Suyama, K.; Arihara, K.; Itoh, M. *Bioresour. Technol.* **2002**, *81*, 201−206.
(6) Ngah, W. S. W.; Liang, K. H. *Ind. Eng. Chem. Res.* **1999**, *38*, 1411−1414.
(7) Ott, I. *Coord. Chem. Rev.* **2009**, *253*, 1670−1681.
(8) Mohamed, A. A.; Chen, J.; Bruce, A. E.; Bruce, M. R.; Krause Bauer, J. A.; Hill, D. T. *Inorg. Chem.* **2003**, *42*, 2203−2205.
(9) Shaw, C. F. *Chem. Rev.* **1999**, *99*, 2589−2600.
(10) Messori, L.; Marcon, G. *Met. Ions Biol. Syst.* **2004**, *41*, 279−304.
(11) Sardar, R.; Funston, A. M.; Mulvaney, P.; Murray, R. W. *Langmuir* **2009**, *25*, 13840−13851.
(12) Murphy, C. J.; Gole, A. M.; Stone, J. W.; Sisco, P. N.; Alkilany, A. M.; Goldsmith, E. C.; Baxter, S. C. *Acc. Chem. Res.* **2008**, *41*, 1721−1730.
(13) Tsoutsi, D.; Guerrini, L.; Hermida-Ramon, H. M.; Giannini, V.; Liz-Marzán, L. M.; Wei, A.; Alvarez-Puebla, R. A. *Nanoscale* **2013**, *5*, 5841−5846.
(14) Gómez-Graña, S.; Pérez-Juste, J.; Alvarez-Puebla, R. A.; Guerrero-Martínez, A.; Liz-Marzán, L. M. *Adv. Opt. Mater.* **2013**, *7*, 477−481.
(15) Goodman, C. M.; McCusker, C. D.; Yilmaz, T.; Rotello, V. M. *Bioconjugate Chem.* **2004**, *15*, 897−900.
(16) Nyarko, E.; Hara, T.; Grab, D. J.; Habib, A.; Kim, Y.; Nikolskaia, O.; Fukuma, T.; Tabata, M. *Chem.-Biol. Interact.* **2004**, *148*, 19−25.
(17) Goebel, C.; Kubicka-Muranyi, M.; Tonn, T.; Gonzalez, J.; Gleichmann, E. *Arch. Toxicol.* **1995**, *69*, 450−459.
(18) Parkinson, J.; Sadler, P. *Chem. Commun.* **1999**, 1359−1360.
(19) Habib, A.; Tabata, M. J. *Inorg. Biochem.* **2004**, *98*, 1696−1702.
(20) Park, J.; Choi, S.; Kim, T.-I.; Kim, Y. *Analyst* **2012**, *137*, 4411−4414.
(21) Kundu, A.; Layek, R. K.; Kuila, A.; Nandi, A. K. *ACS Appl. Mater. Interfaces* **2012**, *4*, 5576−5582.
(22) Yang, Y.; Yin, C.; Huo, F.; Chao, J. *RSC Adv.* **2013**, *3*, 9637−9640.
(23) Connor, E. E.; Mwamuka, J.; Gole, A.; Murphy, C. J.; Wyatt, M. D. *Small* **2005**, *1*, 325−327.
(24) Butler, O. T.; Cook, J. M.; Harrington, C. F.; Hill, S. J.; Rieuwerts, J.; Miles, D. L. *J. Anal. At. Spectrom.* **2007**, *22*, 187−221.
(25) Hung, Y.-L.; Hsiung, T.-M.; Chen, Y.-Y.; Huang, Y.-F.; Huang, C.-C. *J. Phys. Chem. C* **2010**, *114*, 16329−16334.
(26) Egorova, O. A.; Seo, H.; Chatterjee, A.; Ahn, K. H. *Org. Lett.* **2009**, *12*, 401−403.
(27) Do, J. H.; Kim, H. N.; Yoon, J.; Kim, J. S.; Kim, H.-J. *Org. Lett.* **2010**, *12*, 932−934.
(28) Dong, M.; Wang, Y.-W.; Peng, Y. *Org. Lett.* **2010**, *12*, 5310−5313.
(29) Zhang, J. F.; Zhou, Y.; Yoon, J.; Kim, J. S. *Chem. Soc. Rev.* **2011**, *40*, 3416−3429.
(30) Yang, Y.-K.; Lee, S.; Tae, J. *Org. Lett.* **2009**, *11*, 5610−5613.
(31) Kumeria, T.; Kurkuri, M. D.; Diener, K. R.; Parkinson, L.; Losic, D. *Biosens. Bioelectron.* **2012**, *35*, 167−173.
(32) Gauglitz, G. *Anal. Bioanal. Chem.* **2005**, *381*, 141−155.
(33) Gauglitz, G.; Brecht, A.; Kraus, G.; Mahm, W. *Sens. Actuators, B* **1993**, *11*, 21−27.
(34) Lin, V. S.-Y.; Motesharei, K.; Dancil, K.-P. S.; Sailor, M. J.; Ghadiri, M. R. *Science* **1997**, *278*, 840−843.
(35) Dancil, K.-P. S.; Greiner, D. P.; Sailor, M. J. *J. Am. Chem. Soc.* **1999**, *121*, 7925−7930.
(36) Janshoff, A.; Dancil, K.-P. S.; Steinem, C.; Greiner, D. P.; Lin, V. S.-Y.; Gurtner, C.; Motesharei, K.; Sailor, M. J.; Ghadiri, M. R. *J. Am. Chem. Soc.* **1998**, *120*, 12108−12116.
(37) Gauglitz, G. *Anal. Bioanal. Chem.* **2010**, *398*, 2363−2372.
(38) Kumeria, T.; Losic, D. *Phys. Status Solidi RRL* **2011**, *5*, 406−408.
(39) Kumeria, T.; Losic, D. *Nanoscale Res. Lett.* **2012**, *7*, 1−10.
(40) Kumeria, T.; Parkinson, L.; Losic, D. *Nanoscale Res. Lett.* **2011**, *6*, 1−7.
(41) Losic, D.; Velleman, L.; Kant, K.; Kumeria, T.; Gulati, K.; Shapter, J. G.; Beattie, D. A.; Simovic, S. *Aust. J. Chem.* **2011**, *64*, 294−301.
(42) Schwartz, M. P.; Alvarez, S. D.; Sailor, M. *J. Anal. Chem.* **2007**, *79*, 327−334.
(43) Kumeria, T.; Gulati, K.; Santos, A.; Losic, D. *ACS Appl. Mater. Interfaces* **2013**, *5*, 5436−5442.
(44) Santos, A.; Kumeria, T.; Losic, D. *Anal. Chem.* **2013**, *85*, 7904−7911.
(45) Santos, A.; Kumeria, T.; Losic, D. *Trends Anal. Chem.* **2013**, *44*, 25−38.
(46) Pan, S.; Rothberg, L. J. *Nano Lett.* **2003**, *3*, 811−814.
(47) Masuda, H.; Fukuda, K. *Science* **1995**, *268*, 1466−1468.
(48) Zhang, F.; Sautter, K.; Larsen, A. M.; Findley, D. A.; Davis, R. C.; Samha, H.; Linford, M. R. *Langmuir* **2010**, *26*, 14648−14654.
(49) Shiraki, H.; Kimura, Y.; Ishii, H.; Ono, S.; Itaya, K.; Niwano, M. *Appl. Surf. Sci.* **2004**, *237*, 369−373.
(50) Wang, J.; Yang, S.; Liu, X.; Ren, S.; Guan, F.; Chen, M. *Appl. Surf. Sci.* **2004**, *221*, 272−280.